Second International Symposium on Marine Propulsors
smp'11, Hamburg, Germany, June 2011

Development of the Trans-Velocity Propellers

Jeng-Lih Hwang, Shang-Sheng Chin, Kuan-Kai Chang, Tu, Chin-Chin

[1]United Ship Design and Development Center (USDDC), Taipei, Taiwan
[2]Department of Systems Engineering and Naval Architecture, National Taiwan Ocean University, Keelung, Taiwan

ABSTRACT

In this paper, the development of a design procedure for designing the trans-velocity propeller is presented. The design goal is to design a propeller not only having a satisfactory performance, but also having consistent performance at different inflow speeds. The trans-velocity foils (or, inflow-adapted foil) are used for the presented propeller, and the trans-velocity foil has been developed by a multi-objective optimization method in the previous research. The feature of this trans-velocity propeller is that it jumps from the non-cavitation condition to the super-cavitation condition at a very narrow speed range; therefore, it operates like a sub-cavitating propeller at low speeds and intermediate speeds, and then transfer to the super-cavitating propeller for high speed operations. In the design procedure, a lifting-line method and a lifting-surface method are first used to obtain the propeller geometry as the traditional propeller design method. That is, the loading distribution is obtained by satisfying the given torque or the given thrust, and the pitch distribution and the camber distribution are then designed based on the loading distribution of the trans-velocity foil. Since the performance of this propeller includes the consideration of the cavitation and different inflow speeds, the viscous flow RANS method is then used for the computations of this initial design. A systematic iteration is then adopted to adjust the blade geometry until the designed propeller reaches the performance requirement at different speeds. The efficiency of trans-velocity propeller is maintained over 67% in the 20 to 40 knots and its performance data was used with the resistance characteristics of the yacht to determine the practicability. The required horsepower and RPM for the propeller compared to the new section propeller are shown in the paper. However, there is still a gap between the actual product, especially in manufacturing and strength of the structure and these will be made for the future improvements.

KEYWORDS

Propeller design, Trans-velocity propellers, RANS

1 INTRODUCTION

Large naval vessels are typically operated in the speed ranges of 5 to 30+ knots. Currently, the US Navy is actively considering designs with speeds up to 40+ knots in the High Speed Sealift and Littoral Combatant Ship（LCS）programs. The fast ferry and coastal patrol markets are also operating and pursuing development of high speed craft in the 40+ knots speed range. Efficient propulsors for high speed ships are therefore in a greater demand.

The super-cavitating propellers or waterjet propulsors are widely used by high speed ships over 35 knots. Fig. 1, presented by Platzer, shows how these propulsors have a better performance at the high speed range, and this figure also shows how these high speed propulsors tend to have less efficiency at lower speeds compared to conventional propellers.

For good propeller performance, conventional propellers are designed to operate without blade surface cavitation. This type of propeller is termed as a sub-cavitating propeller. Operating in a ship wake, the blade surfaces of a these propellers typically start to experience surface cavitation between 25 and 29 knots. When increasing the ship speed more than 5 knots above the surface cavitation inception speed typically result in severe propeller cavitation, and then results in the loss of propeller efficiency (Fig. 1) along with the thrust breakdown, undesirable noise, blade erosion, and ship vibration problems. Most naval ships, however, have both high full power speeds and an endurance range requirement at lower speeds. Without using a hybrid propulsor which the boost propulsors used in combination with conventional propellers, it is difficult to have good propulsive efficiency cross over a speed range of 20 to 40 knots.

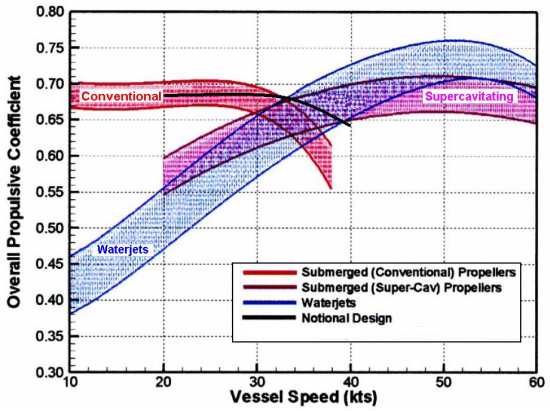

Fig. 1: Overall propulsive coefficient versus ship speed for different propulsor type

2 DESIGN ALGORITHMS

In order to satisfy different design speeds, the design algorithm of a trans-velocity propeller is developed and integrated. We will introduce the design algorithm in this section. The propeller is designed based on the trans-velocity foil, and the design method of the trans-velocity foil has been described by Hwang et al (2009). Three foil design algorithms are developed and integrated in that paper, and they are:

(1) Design a foil based on the given pressure distribution,
(2) Optimize the foil performance based on the Lagrange Multiplier method,
(3) Multi-objective optimization.

A viscous flow RANS method is used for the computation, and the cavitation is also considered in the computations. The optimization problem is to satisfy the lift requirement by minimizing the drag force, and we will describe the multi-objective optimization algorithm used here.

2.1 The design method of the trans-velocity foil

The design method of the trans-velocity foil is based on the Largrange multiplier method. The Lagrange Multiplier method can transfer a constrained problem to a non-constrained problem by introducing the Lagrange multiplier λ. For example, the constrained optimization problem of the foil design problem is to find a two-dimensional foil geometry which provides the minimum drag coefficient (C_D) with a given lift coefficient (C_L). The constraint is therefore $C_L = C_L^*$, and C_L^* is the objective lift coefficient. The design problem thus can be stated as:

$$\begin{cases} \min \quad C_D \\ subject\ to \quad C_L - C_L^* = 0 \end{cases}$$

(1)

We also assume that the lift coefficient and the drag coefficient are functions of angle of attack and geometric parameters. The geometric parameters can be defined by different ways such as camber ratio, thickness, or B-spline control points that defined the foil geometry, etc.:

$$\begin{aligned} C_L &= C_L(\alpha, \gamma_i) \\ C_D &= C_D(\alpha, \gamma_i) \end{aligned} \qquad i = 1,2,3...m$$

(2)

In Equation (2), α is the angle of attack, and , γ_i is the geometric parameters.

We thus can define the Lagrangian of this optimization problem as:

$$L = C_D + \lambda(C_L - C_L^*)$$

(3)

Take the derivatives of Equation (3) with respect to angle of attack, geometric parameters and Lagrange multiplier, and we can obtain:

$$\begin{aligned} &\nabla_V L = \nabla_V C_D + \lambda \nabla_V C_L = 0 \\ &C_L - C_L^* = 0 \end{aligned}$$

(4)

∇_V is defined as the gradient to angle of attack and geometric parameters, and $\nabla_V L$ can be expressed as:

$$\begin{aligned} &\frac{\partial C_D}{\partial \alpha} + \lambda \frac{\partial C_L}{\partial \alpha} \\ &\frac{\partial C_D}{\partial \gamma_i} + \lambda \frac{\partial C_L}{\partial \gamma_i} \end{aligned} \qquad i = 1,2,...,m$$

(5)

This is a non-linear optimization problem, and we define:

$$G = \begin{bmatrix} \nabla_V L \\ C_L - C_L^* \end{bmatrix} \qquad \vec{X} = \begin{bmatrix} \alpha \\ \lambda \\ \vec{\gamma} \end{bmatrix}$$

(6)

where $\vec{\gamma} = [\gamma_1, \gamma_1 ... \gamma_m]^T$ if there are m geometric parameters. The solution of this optimization problem is to solve:

$$G(\vec{X}) = 0$$

(7)

The Newton's method is used to solve this non-linear problem, and we can get:

$$\Delta \vec{X}^j = -\frac{G(\vec{X}^j)}{\nabla G_j}$$

(8)

In Equation (8), the update of $\vec{X}$ is to update the angle of attack, the geometric parameters and the Lagrange multiplier. After an iterative procedure, Equation (8) can be solved, and the design is reached.

The Lagrange Multiplier method described above can be extended to solve a multi-objective problem by introducing a weighting function. For the cases of the "trans-velocity" foil designs, the designed foil has to satisfy the force requirements at different conditions, for example, different speeds or different angles of attack. Therefore, we have the following objective functions and constraints:

$$\begin{cases} \min \quad C_D^k \\ subject\ to \quad C_L^k - C_L^{k*} \geq 0 \end{cases} \qquad k = 1,2,3...$$

(9)

The index k indicates different design conditions. When optimizing the performance of a foil in different conditions, it is not easy to satisfy the same lift requirements. Therefore, usually we can only give the

minimum requirements. For the following constraints:

$$C_L^k - C_L^{k*} \geq 0$$

We can use a slack variable s_k to convert the constraints to:

$$C_L^k - C_L^{k*} - s_k^2 = 0 \quad (10)$$

In order to optimize the foil performance in different conditions, we then introduce a weighting function w, and the Lagrangian of this optimization problem becomes:

$$L = \sum_{k=1}^{N} [w_k C_D^k + \lambda_k (C_L^k - C_L^{k*} - s_k^2)] \quad (11)$$

In Equation (11), the weighting function w is given by the designers by judging the importance of each design condition. We can still follow Equations (4) to (9) to solve this optimization problem except that the slack variables have also to be solved. Equation (4) and Equation (6) thus become the following equations:

$$\nabla_V L = \sum_{k=1}^{N} [w_k \nabla_V C_D^k + \lambda_k \nabla_V C_L^k] = 0$$
$$2\lambda_k s_k = 0$$
$$C_L^k - C_L^{k*} - s_k^2 = 0 \quad (12)$$

We can define:

$$G = \begin{bmatrix} \nabla_V L \\ 2\lambda_k s_k \\ C_L^k - C_L^{k*} - s_k^2 \end{bmatrix}, \qquad \vec{X} = \begin{bmatrix} \alpha \\ \vec{\lambda} \\ \vec{\gamma} \\ \vec{s} \end{bmatrix} \quad (13)$$

where $\vec{\gamma} = [\gamma_1, \gamma_1 \ldots \gamma_m]^T$ if there are m geometric parameters, $\vec{\lambda} = [\lambda_1, \lambda_1 \ldots \lambda_N]^T$ and $\vec{s} = [s_1, s_1 \ldots s_N]^T$ if there are N constraints (N design conditions). Equations (7) and (8) are then used to solve this multi-objective optimization problem.

The multi-objective optimization algorithm described here is a relatively simple method, and it seems to be very effective. However, the total computational time is large since we use the RANS method as the computational method. The final design of the trans-velocity foil is shown in Fig. 2.

2.2 Propeller design based on the trans-velocity foil

Propeller is composed of camber, thickness, pitch, rake, skew and chord length distributions. In the design theory, we mainly design the pitch and camber distributions. The design procedure basically follows the procedure described by Kerwin (1982).

(1) Select the basic propeller geometry such as diameter, hub ratio, blade number and the initial guess distribution of chord length;
(2) Input basic settings such as ship speed, engine speed (RPM) and torque;
(3) The best circulation distribution can be derived by using the lifting line program;
(4) The distribution of the pitch and camber distributions can be derived by using the lifting surface program;
(5) To evaluate whether the torque of designed propeller geometry meets our needs; if the result is expected, the propeller design is to the end; or return to Step 1 to re-adjust the input parameters until the designed geometry meets the required torque.

In the lifting surface design stage, we need the chord-wise loading distribution, and the camber and thickness distributions. All of this information can be obtained from the trans-velocity foil. Fig.2 shows the geometry of the trans-velocity foil, and the camber and thickness distributions decomposed from it.

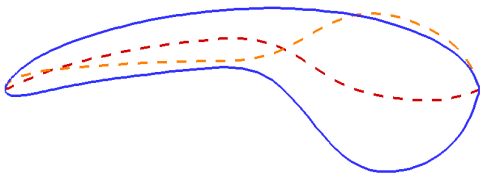

Fig. 2: The camber and thickness distributions of the trans-velocity foil

3 TRANS-VELOCITY PROPELLER DESIGN CASE 1

In this section, we will demonstrate the design of the trans-velocity propeller based on the design procedure described in the last section. The design condition is described as follows:

(1) The blade number is four and the diameter is one meter;
(2) The advanced coefficient is 1.14 and the torque coefficient is 0.0509;
(3) Ship is operated from 20 knot to 40 knot.

We have then designed a propeller according to the design procedure, and the expanded area ratio of the designed propeller is set as 0.667. The performance of this propeller is then evaluated by the viscous flow RANS method. The RANS method we used is the commercial code FLUENT, and the cavitation is taken into consideration. A hybrid grid (un-structure near the propeller surface, and structure in the outer space) are generated and the computational domain is extended one propeller radius to upstream, 2.5 propeller radius

extended to the downstream and radial direction. The set-up of the boundary conditions is shown in Fig. 3. For the propeller cavitation computations, the boundary conditions are set in the same way as the non-cavitating propeller. The only difference is at the exit boundary, where a constant exit pressure is set to match the given cavitation number σ.

The designed propeller geometry is shown as Fig. 4, and according to the computational results, the efficiency is 0.72 at 20 knots, 0.7 at 30 knots and 0.65 at 40 knots. We then investigate the cavitations on the propeller surface, and the condition at J=1.14 and σ=0.098 (40 knots) is computed. The computed iso-surface of vapor volume fraction of 0.5 is shown in Fig. 5. It is observed that the computed cavity shape shows that the propeller is supercavitating; however, the cavity seems not to start from the leading edge, thus we observe the pressure distribution at the 0.5R as shown in Fig. 6. We find the pressure distributions of whole suction side are at the same value as the cavitation number, and this means that the propeller is cavitating from the leading edge. Hence, the iso-surface of vapor volume fraction of 0.5 does not always correspond to the visible cavity observed in photographs. Apparently, more sophisticated modeling and numerical methods on refined grids seem to be required to appropriately capture this type of cavitation.

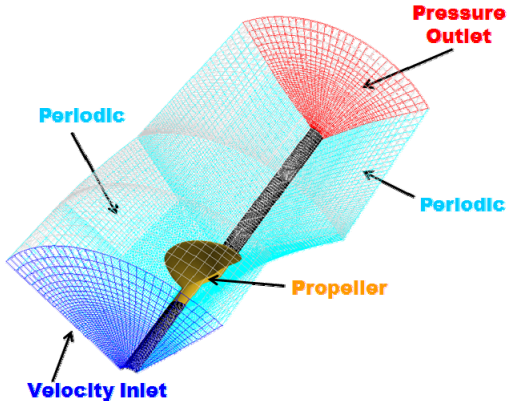

Fig. 3: The computational domain and the boundary conditions used in the RANS computations

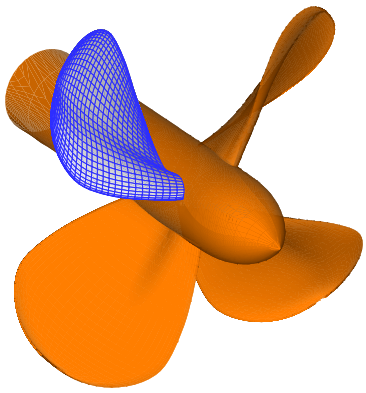

Fig. 4: The computer depiction of the trans-velocity propeller

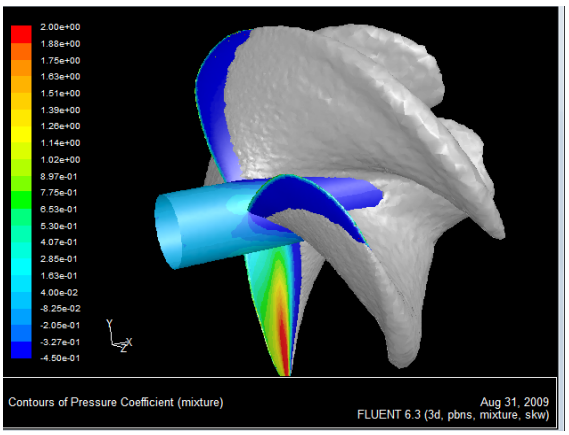

Fig. 5: The computational pressure distribution and the cavitation of the designed propeller at 40 knots

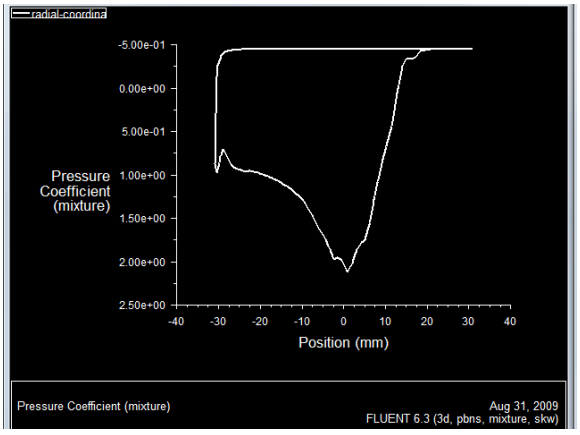

Fig. 6: The pressure distribution at 0.5R of the trans-velocity propeller at 40 knots

Fig. 7 is the complete experimental data of trans-velocity propeller (TVP1) and shows different trends to propeller K-J charts we used to see. Usually, the propeller thrust and torque coefficients will decrease as the cavitation number decreases, but thrust and torque coefficients of this trans-velocity propeller increase while cavitation happened. The reason for this can be explained by the pressure distribution at 0.7R shown in Fig. 8. One can see that there is a convex portion of the pressure distribution after the mid-chord, and this is to create a negative lift to avoid separation at the trailing edge. As the cavitation happened, the negative lift portion can be recovered with the speed increased to 30 knots. Therefore, the thrust and torque coefficient are bigger than non-cavitation. From Fig. 9, we can find that the performance of a “new section” propeller (Kehr 2001) is better than a conventional NACA 66 propeller and the trans-velocity propeller at low and middle speed; however, as the speed gradually increased to more than 35 knots, the TVP1 shows its superiority. The TVP1 propeller also has a relatively stable performance across different speed ranges.

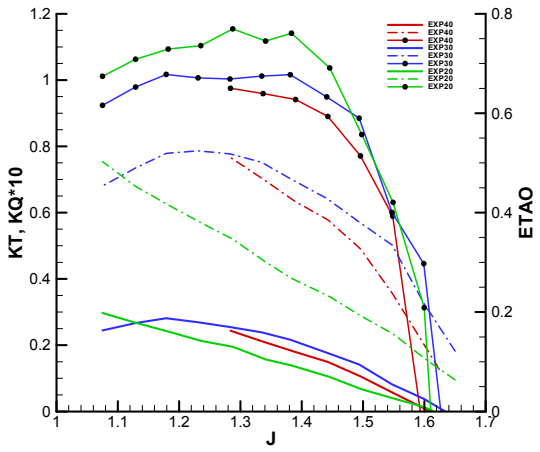

Fig. 7: The complete experimental data of TVP1

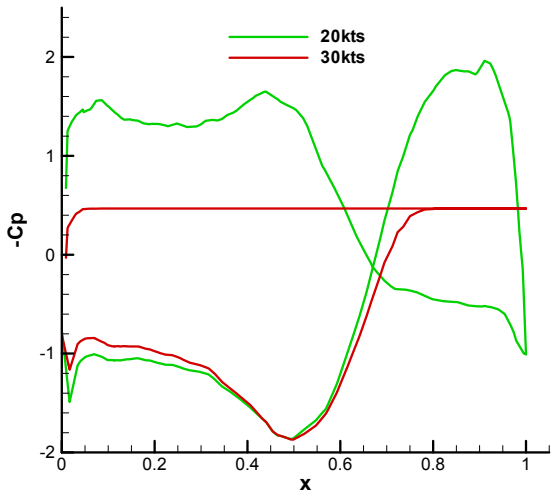

Fig. 8: 0.7R pressure distribution of TVP1 at 20 and 30 knots

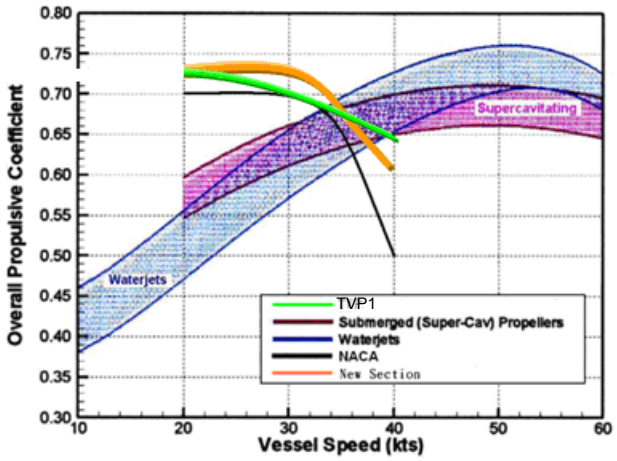

Fig. 9: Efficiency of different propulsors at different speed

4 TRANS-VELOCITY PROPELLER DESIGN CASE 2

From the complete experimental data of trans-velocity propeller, we find the design point shift to 1.35 and over pitch, so that the max propeller torque is bigger than the engine load. We then use the boundary element method to check the torque in the original design process. However, the max propeller torque went along with cavitation, and special geometry makes the boundary element method not able to be estimated correctly. Thus, we used RANS method to check the torque, as in Fig. 10, and designed another trans-velocity propeller. From the circulation distribution calculated by boundary element method (Hsin 2008) and RANS method shown in Fig.11, we know the original design is tip overloaded. We therefore reduce the tip load and modify the pitch and camber to make circulation distribution close to the desired circulation distribution (Fig. 12). Finally, we have obtained a better trans-velocity propeller (TVP2), and the experimental efficiency is 0.72 between 20 to 30 knots and 0.67 at 40 knots. The relatively small drop of the efficiency from 20 knots to 40 knots implies that the influence of the cavitation on the performance of this trans-velocity propeller is not as prominent as conventional propellers.

Fig. 13 shows the comparison of the efficiencies of different propellers at different speeds. We can find that overall the performance of a "new section" propeller is better than a conventional NACA 66 propeller, and the presented trans-velocity propeller (TVP2) is even better than the "new-section" propeller. From the above, we know that the performance of the trans-velocity propeller is as good as a conventional propeller at low or middle speed, and is better than a supercavtation propeller. At high speed, it can smoothly transfer to the supercavitation, and the performance is as good as a supercavitation propeller, and is better than a conventional propeller.

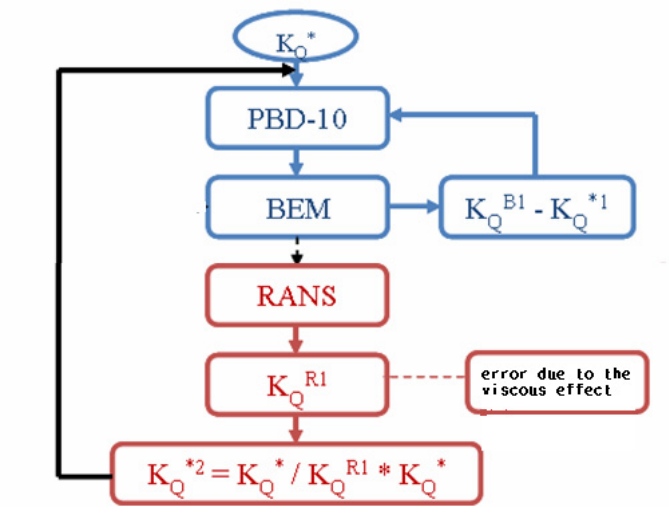

Fig. 10: Modified design process of trans-velocity propeller

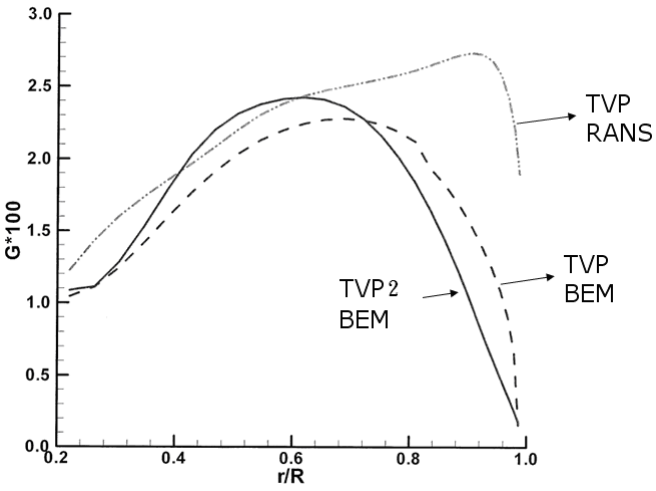

Fig. 11: Circulation distribution calculated by boundary element method and RANS method

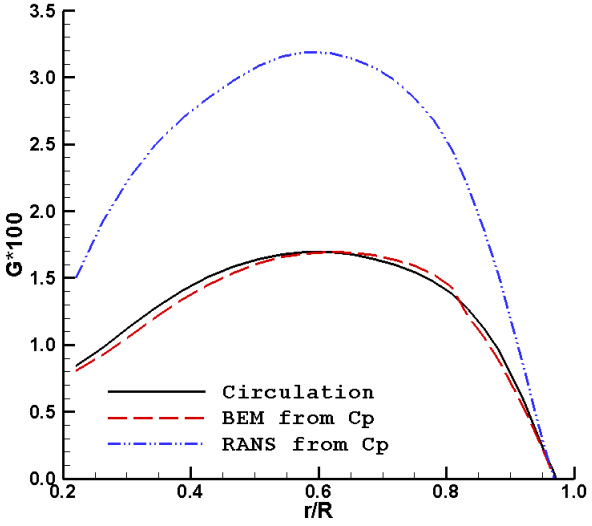

Fig. 12: Circulation distribution of the trans-velocity propeller TVP2

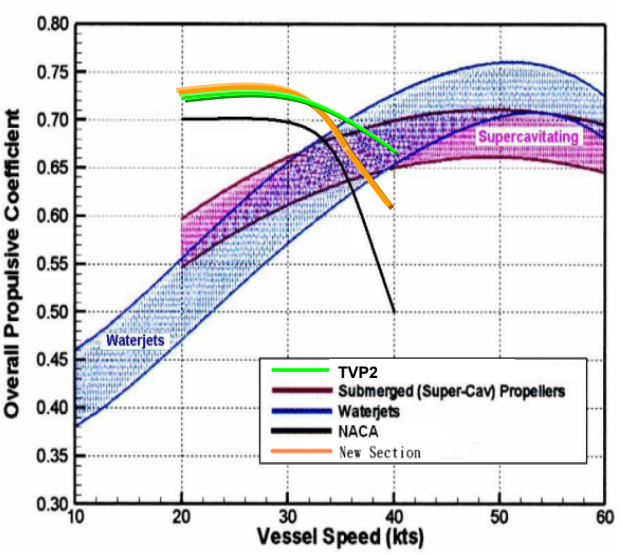

Fig. 13: The superior efficiency of TVP2

In addition to design methods and numerical simulation, we have also tried to understand the practicability of this trans-velocity propeller. We collect the data of effective horse power (EHP) and engine information of a yacht to simulate the installation of this trans-velocity propeller. First, we can get the necessary propeller load from the relationship between ship speed and EHP. Secondly, we can calculate the RPM and BHP with the complete experimental data of trans-velocity propeller. Thirdly, by the engine information, we can estimate the max speed of yacht with propeller installation. In Fig. 14, red curve is the max engine output, green curve is theoretical proposal propeller design trends, yellow curve is the performance of a new section propeller (P4012), and the blue curve is the performance of trans-velocity propeller. According to the experimental data, the max ship speed of the selected yacht with new section propeller is about 35 knots and this trans-velocity propeller can reach 38 knots.

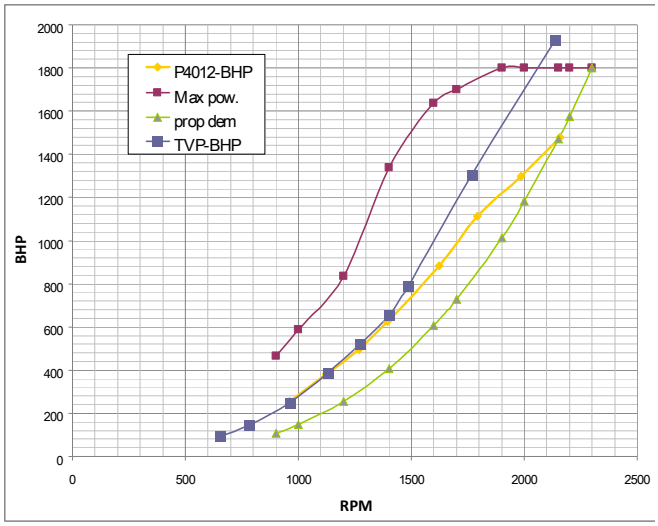

Fig. 14: Relations between RPM and BHP

5 CONCLUSIONS

In this paper, a design procedure for designing the trans-velocity propeller is presented. The design cases show that the design method presented in this paper is effective. However, the designs are very time consuming due to using the viscous flow RANS method. A boundary element method with cavitation model and viscous correction may be more practical, and the RANS method can then be used to verify the final designs.

The trans-velocity propellers designed based on the presented procedure are expected to be operated in a larger range of speeds. Nevertheless, more designs are required to confirm the effectiveness of this design method. Since the trans-velocity propeller will transfer from the non-cavitating condition to the supercavitating condition, the stress analysis of the propeller blade is necessary to verify the structural strength. Also, the blade geometry is more complicated; therefore, we need not only improve the hydrodynamic designs, but also consider the propeller the structure designs and manufacture considerations in the future.

REFERENCES

Hsin, C.-Y., Chang, K.-K., Cheng, Y.-H. & Chang, C.-S. (2008). 'The Analysis and Design of Energy-Saving Propulsors by Computational Methods'. The 3rd Pan Asian Association of Maritime Engineering Societies (3rd PAAMES) and Advanced Maritime Engineering Conference 2008 (AMEC 2008), Chiba, Japan.

Hwang, J. L., Hsin, C. Y., Cheng, Y. H. & Chin, S. S. (2009). 'Design of Inflow-Adapted Foil Sections by Using a Multi-Objective Optimization Method'. smp'09, Trondheim, Norway.

Kehr, Y. Z., Liu, J. H., Li, Y. C. (2001). 'Development of New Section Propeller in High Speed Craft'. 13th SNAME 2001, Taiwan.

Kerwin, J. E. (1982). 'Numerical Method for Propeller Design and Analysis in Steady Flow'. Tran. SNAME.

Liu, D. C., Hong, F. W., Zhao, F. & Zhang, Z. R. (2008). 'The CFD Analysis of Propeller Sheet Cavitation'. Proceeding of 8th ICHD 2008, Nantes, France.

Platzer, G. (2004). 'High Speed Propulsor Alternatives to Waterjet'. ASNE Advanced Naval Propulsion Symposium, Dulles, Virginia.

Rhee, S. H., Kawamura, T. & Li, H. (2005). ,Propeller Cavitation Study Using an Unstructured Grid Based Navier-Stoker Solver'. Journal of Fluids Engineering **127**, pp. 986-994.